USGS
science for a changing world

Petrographic and Geochemical Data for Cenozoic Volcanic Rocks of the Bodie Hills, California and Nevada

Data Series 764
Version 1.1, August 2016

U.S. Department of the Interior
U.S. Geological Survey

Cover: In Bodie Creek, columnar-jointed rhyolite of Bodie Creek (yellowish-tan outcrops on the left side of the photo as well as the darker peak on the skyline) are unconformably overlain by thin, trachyandesite of Beauty Peak lava flows that cap slopes in the middle distance. The rhyolite of Bodie Creek is part of the Miocene Bodie Hills volcanic field, whereas the trachyandesite of Beauty Peak is part of the Pliocene-Pleistocene Aurora volcanic field.

Petrographic and Geochemical Data for Cenozoic Volcanic Rocks of the Bodie Hills, California and Nevada

By Edward A. du Bray, David A. John, Stephen E. Box, Peter G. Vikre, Robert J. Fleck, and Brian L. Cousens

Data Series 764
Version 1.1, August 2016

U.S. Department of the Interior
U.S. Geological Survey

U.S. Department of the Interior
SALLY JEWELL, Secretary

U.S. Geological Survey
Suzette M. Kimball, Director

U.S. Geological Survey, Reston, Virginia
First release: 2013
Revised: August 2016 (ver 1.1)

Suggested citation:
du Bray, E.A., John, D.A., Box, S.E., Vikre, P.G., Fleck, R.J., and Cousens, B.L., 2016, Petrographic and geochemical data for Cenozoic volcanic rocks of the Bodie Hills, California and Nevada (ver. 1.1, August 2016): U.S. Geological Survey Data Series 764, 10 p., http://dx.doi.org/10.3133/ds764.

ISSN 2327-638X (online)

Contents

Introduction....1
Analytical Methods....1
Data Fields....3
Acknowledgments....9
References Cited....9
Appendix 1. Status and Treatment of Samples....link
Appendix 2. Petrographic Data for Rock Samples....link
Appendix 3. Geochemical Data for Rock Samples....link

Figure

1. Index map showing location of the Bodie Hills volcanic field, California and Nevada....2

Tables

1. Definition and characterization of data fields included in appendix 1 (status and treatment of samples)....3
2. Definition and characterization of data fields included in appendix 2 (petrographic data)....5
3. Definition and characterization of data fields included in appendix 3 (geochemical data)....7

Petrographic and Geochemical Data for Cenozoic Volcanic Rocks of the Bodie Hills, California and Nevada

By Edward A. du Bray, David A. John, Stephen E. Box, Peter G. Vikre, Robert J. Fleck, and Brian L. Cousens

Introduction

The purpose of this report is to present available petrographic and geochemical data for unmineralized rock samples, principally volcanic rocks, of the Tertiary Bodie Hills volcanic field and to make those data available to ongoing petrogenetic investigations of these rocks. Most of the data presented here were derived from samples collected between 2000–2013, but some of the geochemical data, compiled from a variety of sources, pertain to samples collected during prior investigations; all samples collected during investigations prior to 2000 are identified by "OTH" in the "Collector" data field (appendix 1). When more than one sample was collected at a sample site, a single representative sample from the site was selected, and only petrographic and geochemical information pertinent to that sample are included in the data compilations that accompany this report.

The middle to late Miocene Bodie Hills volcanic field (BHVF) is a large (>700 km^2), long-lived (≈9 million years [m.y.]), but episodic, eruptive center (John and others, 2012) in the southern segment of the ancestral Cascades arc north of Mono Lake, California (fig. 1). The field is near the west side of the Walker Lane and the northwest end of the Mina deflection where structures related to these tectonic features might have localized BHVF magmatism. The BHVF includes at least 32 volcanic rock units. The field includes four trachyandesite stratovolcanoes that were emplaced along its margins and numerous silicic trachyandesite to rhyolite flow dome complexes that were generally localized more centrally. Volcanism in the BHVF was discontinuous through time, with two peak periods of eruptive activity, including an early period between ≈15.0 to 12.6 Mega-annum (Ma) that formed large stratovolcanoes and a later period between ≈9.9 to 8.0 Ma dominated by emplacement of large silicic trachyandesite-dacite lava domes. A final period of small-volume silicic dome emplacement occurred at about 6 Ma.

Compositions of Bodie Hills volcanic rocks vary from ≈50 to 78 weight percent SiO_2, although rocks with <55 weight percent SiO_2 are rare. Rock compositions form a high-potassium (K) calc-alkaline series with pronounced negative titanium-phosphorus-niobium-tantalum anomalies and high barium/niobium, barium/tantalum, and lanthanum/niobium typical of subduction-related continental margin arcs (Gill, 1981). Most BHVF rocks are porphyritic, commonly containing 15–35 volume percent phenocrysts of plagioclase, pyroxene, and hornblende ±biotite. Although the oldest eruptive centers have the most mafic compositions, erupted rock compositions oscillated between mafic and intermediate to felsic compositions through time. Following a 2 m.y. hiatus in volcanism, post subduction rocks of the ≈3.9- to 0.1-Ma, bimodal, high-K Aurora volcanic field were erupted onto the BHVF. Formation of the Bodie Hills volcanic field spanned the transition between subduction of the Farallon plate beneath the west coast of North America and the establishment of a transform plate margin at about 10 Ma. However, significant volcanism in the Bodie Hills persisted to 8 Ma without apparent changes in rock composition or style of eruption.

Numerous hydrothermal systems were operative in the Bodie Hills during the Miocene. Structurally focused hydrothermal systems formed large epithermal gold-silver vein deposits in the Bodie and Aurora mining districts. Economically important hydrothermal systems in the Bodie Hills are temporally related to intermediate- to silicic-composition dome complexes (John and others, 2012).

Analytical Methods

Standard petrographic microscope techniques were employed to identify phenocryst minerals and estimate their relative abundances in 706 samples of volcanic rocks from the Bodie Hills (appendix 2; see **Data Fields**, below). Phenocryst size and crystallinity, rock textures, groundmass characteristics, and accessory mineral assemblages were also tabulated for each sample. Characteristics of the Mesozoic basement rocks, including granitoids of the Sierra Nevada batholith and their metamorphic host rocks, were also established by reconnaissance petrographic study of 31 samples. Relative mineral abundances in 20 Mesozoic granitoid rock samples were further refined using a binocular microscope to count at least 1,000 points on slabs stained using the method of Laniz and others (1964). Additional petrographic characteristics for 21 samples of the Aurora volcanic field were compiled from the literature (Lange and Carmichael, 1996).

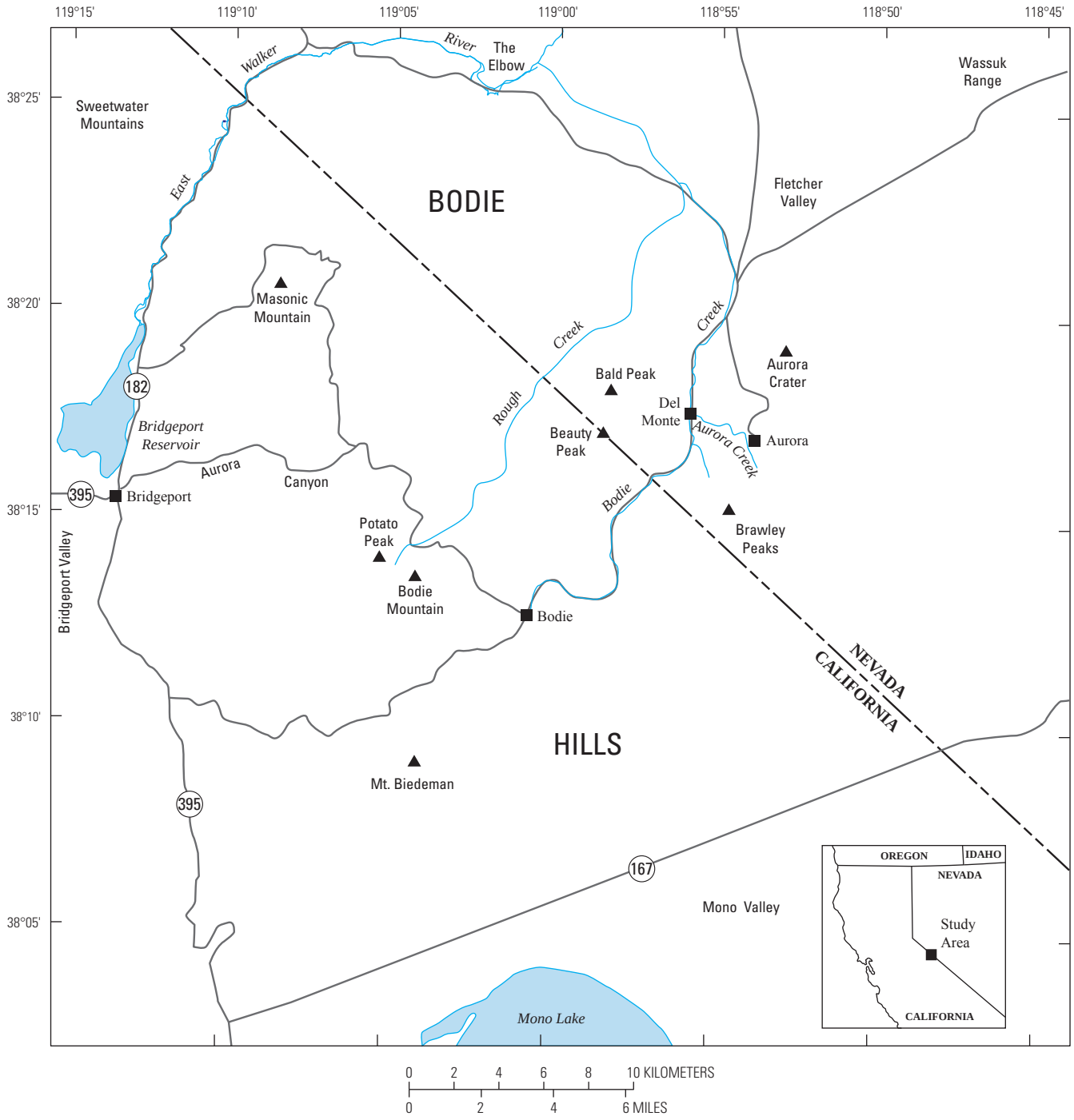

Figure 1. Index map showing location of the Bodie Hills volcanic field, California and Nevada

Whole-rock chemical analyses (556 samples) for samples collected between 2000 and 2013 were performed in analytical laboratories of SGS Minerals, Toronto, Canada (appendix 3; see **Data Fields**, below). Major oxide abundances (recalculated to 100 percent, volatile-free) were determined by wavelength dispersive X-ray fluorescence spectrometry. A 55-element method that uses a combination of inductively coupled plasma–atomic emission spectrometry and inductively coupled plasma–mass spectrometry was used to determine trace element abundances. These chemical data are also archived in the National Geochemical Database (U.S. Geological Survey, 2008). Pertinent analytical methods are described by Taggart (2002). Compositions of an additional 109 samples of Bodie Hills rocks from published sources are included in this data compilation. These samples were analyzed by different laboratories employing diverse analytical techniques, which resulted in data of variable quality for a highly variable set of constituents. Laboratories, techniques, and the analyzed constituents are documented in the sources (identified in appendix 1; see **Data Fields**, below) from which these data were compiled.

Although every effort was made to collect only unaltered samples, a review of the geochemical data indicates that a small subset of the analyzed samples were affected by post-magmatic hydrothermal alteration. Samples with any of the following characteristics are considered to be altered: SiO_2 abundances greater than 78 percent, volatile (loss on ignition) content greater than 4 percent (excluding hydrated vitrophyres), Na_2O abundances less than 1 percent, K_2O abundances greater than 7.5 percent, or Na_2O/K_2O less than 0.5. Primary igneous rock compositions of samples with any of these characteristics probably have not been preserved; these samples and the type of alteration they experienced are identified by entries in the Alt_Desc column in appendix 1. In addition, samples with initial analytic totals less than 98 percent probably indicate inaccurate analyses (see entries in the total_I_pct column of appendix 3).

Data Fields

Sample characterization, petrographic, and geochemical data are presented in columns or sets of related columns (appendixes 1, 2, and 3) in three Microsoft Excel 2003 workbooks (.xls format). The contents of appendix 1 (data fields defined in table 1) constitute basic characterization including sample location, sample treatment, lithologic characterization for each sample, and age of the unit represented by each sample. Appendix 2 contains petrographic observations for each sample (data fields defined in table 2). Appendix 3 contains geochemical data for analyzed samples (data fields defined in table 3). Geochemical data in some worksheet cells may appear to be more precise than displayed values, but the implied precision is a misleading artifact of computational processes (for instance, recalculation to 100-percent volatile free) used to create data-cell contents. Blank cells in the worksheet appendixes indicate null values or that no data are available. In appendix 3 (geochemistry data), some blank cells reflect abundances that were reported as “less than the detection limit”; these values were replaced by blank cells to enable statistical analysis of the uncensored data.

Table 1. Definition and characterization of data fields included in appendix 1 (status and treatment of samples).

FIELD_NAME	FIELD_DESCRIPTION
Field_ID	Field-assigned sample identifier; Field_ID entries link data for individual rows to the contents of particular rows in the other appendixes and, for USGS samples, to the National Geochemical Database.
Collector	Sample collector initials, where EDB is E.A. du Bray, DAJ is D.A. John, JJR is J.J. Rytuba, PGV is P.G. Vikre, SEB is S.E. Box, RJF is R.J. Fleck, OTH is other (as identified in the Chem_Src field), KC is Susan Kingdon and Brian Cousens, and MAC is M.A. Cosca.
EquivSpl	Co-located sample(s)
Longitude	In decimal degrees, relative to the North American Datum of 1927; locations (with four or five significant figures) of samples collected between 2000 and 2012 were determined using global positioning system technology and are accurate within several to tens of meters, whereas locations (with two or three significant figures) of some previously collected samples are accurate within hundreds of meters. Longitude is reported as a negative value (western hemisphere).
Latitude	In decimal degrees, relative to the North American Datum of 1927; locations (with four or five significant figures) of samples collected between 2000 and 2012 were determined using global positioning system technology and are accurate within several to tens of meters, whereas locations (with two or three significant figures) of some previously collected samples are accurate within hundreds of meters. Latitude as a positive value (northern hemisphere).
Chem	X, chemical analysis for sample obtained (see appendix 3)
TS	X, thin section of sample prepared and examined using a petrographic microscope (see appendix 2)
PTS	X, polished thin section of sample prepared and examined using a petrographic microscope (see appendix 2)

Table 1. Definition and characterization of data fields included in appendix 1 (status and treatment of samples).—Continued

FIELD_NAME	FIELD_DESCRIPTION
REF	X, reference sample collected; SS, stained slab of Mesozoic granitoid samples prepared for modal analysis (see appendix 2)
Ar_Ar	X, sample age determined by $^{40}Ar/^{39}Ar$ geochronology (John and others, 2012)
Isotope	X, radiogenic Sr, Pb, and Nd isotope data obtained for sample (unpublished data)
Fe_TiOx	X, Fe-Ti oxide mineral compositions (not included in database) determined via microprobe analysis (unpublished data)
Strat_Name	Stratigraphic unit name (John and others, 2012)
Lithology	All volcanic rock composition names were established using the total alkalis versus silica nomenclature grid (Le Bas and others, 1986); in accordance with procedures defined by the International Union of Geological Sciences, composition names for intrusive rocks are defined using the relative modal proportions of quartz, alkali feldspar, and plagioclase relative to the classification scheme of Streckeisen (1976).
Ign_Form	Form (lava, ash-flow tuff, plug, stock, and so forth) of the igneous rock represented by each sample
Alt_Desc	Terms used to characterize altered samples are secondary silica, hydrated glass (where hydration is extensive), loss on ignition greater than 4, potassic, propylitic, silicified, total less than 98, argillic, and alkali metasomatism; terms are applied in accordance with their standard usage, defined for instance by Guilbert and Park (1986).
Chem_Src	Source of chemical data: 1, O'Neil and others (1973); 2, Al-Rawi (1969); 3,Chesterman and others (1986); 4, du Bray, E.A., John, D.A., Box, S.E., and Vikre, P.G., U.S. Geological Survey, unpublished data (2012); 5, Silberman and Chesterman (1995); 6, U.S. Geological Survey (2008); 7, Ormerod (1988); 8, Lange and Carmichael (1996); 9, Osborne (1985); 10, Putirka, Keith, California State University, Fresno, unpublished data (2008); 11, Kingdon (2016); for a few samples, data were culled from two or more sources; for example, major oxide data may have been compiled from one source and trace element data from another.
Rad_Age	Radiometric age, in million years; in some instances, multiple geochronologic age determinations have been obtained for a single sample; all multiple ages are separated by semi-colons.
Uncert	Age analytical uncertainty, in million years, associated with age determinations reported in "Rad_Age"
Age_Src	Source of age data: A, Silberman and Chesterman (1972); B, Silberman and McKee (1972); C, Fleck and others (2015); D, Gilbert and others (1968); E, Lange and others (1993)
Age	Sample age, in Mega-annum, based on cited age determinations or estimated from ages determined for other samples of the identified stratigraphic unit; empty cells indicate samples and corresponding stratigraphic units for which definitive ages are lacking.

Table 2. Definition and characterization of data fields included in appendix 2 (petrographic data).

FIELD_NAME	FIELD_DESCRIPTION
Field_ID	Field-assigned sample identifier; Field_ID entries link data for individual rows to the contents of particular rows in the other appendices and, for USGS samples, to the National Geochemical Database
Strat_Name	Stratigraphic unit name (John and others, 2012); repeated in this appendix to enable data sorting by unit name
AbdQtz	Microscope-based estimate of abundance of quartz relative to the whole rock, in volume percent. TR, trace (<0.5 volume percent) amounts; abd, abundant (≥20 volume percent); X, present; ?, presence uncertain
AbdAlkFld	Microscope-based estimate of abundance of alkali feldspar relative to the whole rock, in volume percent. TR, trace (<0.5 volume percent) amounts; abd, abundant (≥20 volume percent); X, present
AbdPl	Microscope-based estimate of abundance of plagioclase relative to the whole rock, in volume percent TR, trace (<0.5 volume percent) amounts; abd, abundant (≥20 volume percent); X, present
AbdHbl	Microscope-based estimate of abundance of hornblende relative to the whole rock, in volume percent. TR, trace (<0.5 volume percent) amounts; ??, presence uncertain
AbdBt	Microscope-based estimate of abundance of biotite relative to the whole rock, in volume percent; TR, trace (<0.5 volume percent) amounts
AbdPx	Microscope-based estimate of abundance of pyroxene relative to the whole rock, in volume percent; TR, trace (<0.5 volume percent) amounts
Cpx_Opx	Presence of clinopyroxene (C) and orthopyroxene (O); if both are present, then letter designation for dominant pyroxene is uppercase, and letter designation for subordinate pyroxene follows in lower case; if both are capitalized the two pyroxenes are approximately equally abundant
AbdOl	Microscope-based estimate of abundance of olivine relative to the whole rock, in volume percent. TR, trace (<0.5 volume percent) amounts; ??, presence uncertain
AbdOpq	Microscope-based estimate of abundance of opaque iron-titanium oxide minerals relative to the whole rock, in volume percent. TR, trace (<0.5 volume percent) amounts; X, present; ?, presence uncertain
TotXls	Microscope-based estimate of total phenocryst content relative to the whole rock, in volume percent; TR, trace (<0.5 volume percent) amounts
ClrIndx	Microscope-based estimate of color index (sum of the abundances of hornblende, biotite, pyroxene, olivine, and opaque iron-titanium oxide minerals) in volume percent; TR, trace (<0.5 volume percent) amounts
AgsQtz	Microscope-based estimate of average grain size of quartz phenocrysts, in millimeters
AgsAlkFld	Microscope-based estimate of average grain size of alkali feldspar phenocrysts, in millimeters
AgsPl	Microscope-based estimate of average grain size of plagioclase phenocrysts, in millimeters
AgsHbl	Microscope-based estimate of average grain size of hornblende phenocrysts, in millimeters
AgsBt	Microscope-based estimate of average grain size of biotite phenocrysts, in millimeters
AgsPx	Microscope-based estimate of average grain size of pyroxene phenocrysts, in millimeters
AgsOl	Microscope-based estimate of average grain size of olivine phenocrysts, in millimeters
AgsOpq	Microscope-based estimate of average grain size of opaque iron-titanium oxide phenocrysts, in millimeters
MgsQtz	Microscope-based estimate of maximum grain size (length) of largest quartz phenocryst, in millimeters
MgsAlkFld	Microscope-based estimate of maximum grain size (length) of largest alkali feldspar phenocryst, in millimeters
MgsPl	Microscope-based estimate of maximum grain size (length) of largest plagioclase phenocryst, in millimeters
MgsHbl	Microscope-based estimate of maximum grain size (length) of largest hornblende phenocryst, in millimeters
MgsBt	Microscope-based estimate of maximum grain size (length) of largest biotite phenocryst, in millimeters
MgsPx	Microscope-based estimate of maximum grain size (length) of largest pyroxene phenocryst, in millimeters
MgsOl	Microscope-based estimate of maximum grain size (length) of largest olivine phenocryst, in millimeters
MgsOpq	Microscope-based estimate of maximum grain size (length) of largest opaque iron-titanium oxide phenocryst, in millimeters
Texture	Characteristic petrographic textures as determined by microscopic observation—abbreviations: A, aphyric; APH, aphanitic; F, fragmental; fine grnd, fine grained; FL, flow laminated; H, hyalophitic; HC, holocrystalline; HG, hypidiomorphic granular; I, intersertal; IG, intergranular; IN, inequigranular; med grnd, medium-grained; P, porphyritic; PT, pilotaxitic; S, seriate; SPH, spherulitic; T, trachytic; V, vesicular; X, xenomorphic

Table 2. Definition and characterization of data fields included in appendix 2 (petrographic data).—Continued

FIELD_NAME	FIELD_DESCRIPTION
AccessMnrls	Accessory minerals identified by microscopic observation; listed in order of decreasing abundance—abbreviations: Aln, allanite; Ap, apatite; Ttn, titanite; Zrn, zircon
XlQtz	Microscope-based estimate of crystallinity of quartz phenocrysts—abbreviations: A, anhedral; S, subhedral; E, euhedral. If more than one crystallinity type is present, the dominant form is listed first.
XlAlkFld	Microscope-based estimate of crystallinity of alkali feldspar phenocrysts—abbreviations: A, anhedral; S, subhedral; E, euhedral. If more than one crystallinity type is present, the dominant form is listed first.
XlPl	Microscope-based estimate of crystallinity of plagioclase phenocrysts—abbreviations: A, anhedral; S, subhedral; E, euhedral. If more than one crystallinity type is present, the dominant form is listed first.
XlHbl	Microscope-based estimate of crystallinity of hornblende phenocrysts—abbreviations: A, anhedral; S, subhedral; E, euhedral. If more than one crystallinity type is present, the dominant form is listed first.
XlBt	Microscope-based estimate of crystallinity of biotite phenocrysts—abbreviations: A, anhedral; S, subhedral; E, euhedral. If more than one crystallinity type is present, the dominant form is listed first.
XlPx	Microscope-based estimate of crystallinity of pyroxene phenocrysts—abbreviations: A, anhedral; S, subhedral; E, euhedral. If more than one crystallinity type is present, the dominant form is listed first.
XlOl	Microscope-based estimate of crystallinity of olivine phenocrysts—abbreviations: A, anhedral; S, subhedral; E, euhedral. If more than one crystallinity type is present, the dominant form is listed first.
XlOpq	Microscope-based estimate of crystallinity of opaque iron-titanium oxide phenocrysts—abbreviations: A, anhedral; S, subhedral; E, euhedral. If more than one crystallinity type is present, the dominant form is listed first.
Petrog_Com	Groundmass (gndms) characteristics and any otherwise noteworthy features; the degree to which hornblende (Hbl) and biotite (Bi) are oxidized is also noted
HblClr	Pleochroic colors of hornblende phenocrysts, if present
AltExtnt	Microscope-based estimate of the extent of alteration where 1 indicates a completely fresh sample and 5 indicates a completely altered sample in which primary textures and minerals are not identifiable; intermediate values of 2 through 4 identify progressively more altered samples.

Table 3. Definition and characterization of data fields included in appendix 3 (geochemical data).

FIELD_NAME	FIELD_DESCRIPTION
Field_ID	Field-assigned sample identifier; Field_ID entries link data for individual rows to the contents of particular rows in the other appendices and, for USGS samples, to the National Geochemical Database
Strat_Name	Stratigraphic unit name (John and others, 2012); repeated in this appendix to enable data sorting by unit name
SiO2_pct	Silicon, as silicon dioxide, in weight percent; recalculated to 100 percent on a volatile-free basis
TiO2_pct	Titanium, as titanium dioxide, in weight percent; recalculated to 100 percent on a volatile-free basis
Al2O3_pct	Aluminum, as aluminum trioxide, in weight percent; recalculated to 100 percent on a volatile-free basis
FeO*_pct	Total iron, as ferrous oxide, in weight percent; recalculated to 100 percent on a volatile-free basis
MnO_pct	Manganese, as manganese oxide, in weight percent; recalculated to 100 percent on a volatile-free basis
MgO_pct	Magnesium, as magnesium oxide, in weight percent; recalculated to 100 percent on a volatile-free basis
CaO_pct	Calcium, as calcium oxide, in weight percent; recalculated to 100 percent on a volatile-free basis
Na2O_pct	Sodium, as sodium oxide, in weight percent; recalculated to 100 percent on a volatile-free basis
K2O_pct	Potassium, as potassium oxide, in weight percent; recalculated to 100 percent on a volatile-free basis
P2O5_pct	Phosphorus, as phosphorus pentoxide, in weight percent; recalculated to 100 percent on a volatile-free basis
LOI_pct	Volatile content lost on ignition, in weight percent
H2Ob_pct	Structurally bound or essential water, in weight percent
H2Om_pct	Nonessential moisture, in weight percent
CO2_pct	Carbon dioxide, in weight percent
F_pct	Fluoride, in weight percent
Total_I_pct	Initial, pre-recalculation sum of oxide abundances, in weight percent
Volatile_pct	Total volatile content, in weight percent; calculated as the sum of moisture, bound water and carbon dioxide, or as the content lost on ignition
Ba_ppm	Barium, in parts per million
Be_ppm	Beryllium, in parts per million
Cs_ppm	Cesium, in parts per million
Rb_ppm	Rubidium, in parts per million
Sr_ppm	Strontium, in parts per million
Y_ppm	Yttrium, in parts per million
Zr_ppm	Zirconium, in parts per million
Hf_ppm	Hafnium, in parts per million
Th_ppm	Thorium, in parts per million
U_ppm	Uranium, in parts per million
Ga_ppm	Gallium, in parts per million
La_ppm	Lanthanum, in parts per million
Ce_ppm	Cerium, in parts per million
Pr_ppm	Praeseodymium, in parts per million
Nd_ppm	Neodymium, in parts per million
Sm_ppm	Samarium, in parts per million
Eu_ppm	Europium, in parts per million
Gd_ppm	Gadolinium, in parts per million
Tb_ppm	Terbium, in parts per million
Dy_ppm	Dysprosium, in parts per million
Ho_ppm	Holmium, in parts per million
Er_ppm	Erbium, in parts per million
Tm_ppm	Thulium, in parts per million
Yb_ppm	Ytterbium, in parts per million

Table 3. Definition and characterization of data fields included in appendix 3 (geochemical data).—Continued

FIELD_NAME	FIELD_DESCRIPTION
Lu_ppm	Lutetium, in parts per million
Ag_ppm	Silver, in parts per million
Au_ppm	Gold, in parts per million
Co_ppm	Cobalt, in parts per million
Cr_ppm	Chromium, in parts per million
Ni_ppm	Nickel, in parts per million
Sc_ppm	Scandium, in parts per million
V_ppm	Vanadium, in parts per million
Cu_ppm	Copper, in parts per million
Mo_ppm	Molybdenum, in parts per million
Pb_ppm	Lead, in parts per million
Zn_ppm	Zinc, in parts per million
Sn_ppm	Tin, in parts per million
W_ppm	Tungsten, in parts per million
Ta_ppm	Tantalum, in parts per million
As_ppm	Arsenic, in parts per million
Sb_ppm	Antimony, in parts per million
B_ppm	Boron, in parts per million
Delta_18O	1,000 times the stable isotope ratio of ^{18}O to ^{16}O relative to the same ratio in a standard (usually SMOW, standard mean ocean water) minus 1, in parts per thousand (per mil)
87Sr_86Sr_I	Initial isotope ratio of ^{87}Sr (generated by radioactive decay of ^{87}Rb) to ^{86}Sr; except data from Ormerod (1988) (Age_Src=7), which are measured $^{87}Sr/^{86}Sr$ ratios; initial ratios are calculated from measured $^{87}Sr/^{86}Sr$ ratios and assigned sample ages based on radiometric dating of units
206Pb_204Pb	Isotope ratio of ^{206}Pb (generated by radioactive decay of ^{238}U) to ^{204}Pb
207Pb_204Pb	Isotope ratio of ^{207}Pb (generated by radioactive decay of ^{235}U) to ^{204}Pb
208Pb_204Pb	Isotope ratio of ^{208}Pb (generated by radioactive decay of ^{232}Th) to ^{204}Pb
143Nd_144Nd	Isotope ratio of ^{143}Nd (generated by radioactive decay of ^{147}Sm) to ^{144}Nd

Acknowledgments

Geologic mapping and sample collection for this study were conducted as part of the Mineral Systems of the Ancestral and Modern Cenozoic Cascades Arcs Project funded by the U.S. Geological Survey Mineral Resources Program. Constructive reviews by Matthew Granitto and S.M. Smith are much appreciated and helped clarify data presentation.

References Cited

Al-Rawi, Y.T., 1969, Cenozoic history of the northern part of Mono Basin (Mono County), California and Nevada: Berkeley, Calif., University of California, Ph. D. dissertation, 163 p.

Chesterman, C.W., Chapman, R.H., and Gray, C.H., Jr., 1986, Geology and ore deposits of the Bodie mining district, Mono County, California: California Division of Mines and Geology Bulletin 206, 35 p.

Fleck, R.J., du Bray, E.A., John, D.A., Vikre, P.G., Cosca, M.A., Snee, L.W., and Box, S.E., 2015, Geochronology of Cenozoic rocks in the Bodie Hills, California and Nevada: U.S. Geological Survey Data Series 916, 26 p., http://dx.doi.org/10.3133/ds916.

Gilbert, C.M., Christiansen, M.N., Al-Rawi, Yehya, and Lajoie, K.R., 1968, Structural and volcanic history of Mono Basin, California-Nevada, *in* Coats, R.R., Hay, R.L., and Anderson, C.A., eds., Studies in volcanology: Geological Society of America Memoir 116, p. 275–329.

Gill, J., 1981, Orogenic andesites and plate tectonics: New York, Springer-Verlag, 390 p.

Guilbert, J.M., and Park, C.F., Jr., 1986, The geology of ore deposits: New York, Freeman, 985 p.

John, D.A., du Bray, E.A., Fleck, R.J., Vikre, P.G., Box, S.E., and Moring, B.C., 2012, Miocene magmatism in the Bodie Hills volcanic field, California and Nevada: A long-lived eruptive center in the southern segment of the ancestral Cascades arc: Geosphere, v. 8, p. 44–97.

Kingdon, S.A., 2016, Pliocene to late Pleistocene magmatism in the Aurora Volcanic Field Nevada and California, USA—A petrographic, geochemical, and isotopic study: Ottawa, Canada, Carlton University, Masters thesis, 229 p.

Lange, R.A., and Carmichael, I.S.E., 1996, The Aurora volcanic field, California-Nevada: Oxygen fugacity constraints on the development of andesitic magma: Contributions to Mineralogy and Petrology, v. 125, p. 167–185.

Lange, R.A., Carmichael, I.S.E., and Renne, Paul, 1993, Potassic volcanism near Mono Basin, California: Evidence for high water and oxygen fugacities inherited from subduction: Geology, v. 21, p. 949–952.

Laniz, R.V., Stevens, R.E., and Norman, M.B., 1964, Staining of plagioclase feldspar and other minerals with F.D. and C. red no. 2: U. S. Geological Survey Professional Paper 501-B, p. B152–B153.

Le Bas, M.J., Le Maitre, R.W., Streckeisen, Albert, and Zanettin, Bruno, 1986, A chemical classification of volcanic rocks using the total alkali-silica diagram: Journal of Petrology, v. 27, p. 745–750.

O'Neil, J.R., Silberman, M.L., Fabbi, B.P., and Chesterman, C.W., 1973, Stable isotope and chemical relations during mineralization in the Bodie mining district, Mono County, California: Economic Geology, v. 68, p. 765–784.

Ormerod, D.S., 1988, Late- to post-subduction magmatic transitions in the western Great Basin, U.S.A: Milton Keynes, United Kingdom, Open University, Ph. D. dissertation, 331 p.

Osborne, M.A., 1985, Alteration and mineralization of the northern half of the Aurora mining district, Mineral County, Nevada: Reno, Nevada, University of Nevada, M.S. thesis, 93 p.

Silberman, M.L., and Chesterman, C.W., 1972, K-Ar age of volcanism and mineralization, Bodie mining district and Bodie Hills volcanic field, Mono County, California: Isochron/West, no. 3, p. 13–22.

Silberman, M.L., and Chesterman, C.W., 1995, A description of the Bodie Hills and Bodie mining district, Mono County, California, *in* Jones, Elizabeth, ed., Geology and ore deposits of Bodie Hills, northern Mono Basin region; Bodie Hills, Aurora district: Geological Society of Nevada Special Publication, v. 22, p. 2–8.

Silberman, M.L., and McKee, E.H., 1972, A summary of radiometric age determinations on Tertiary volcanic rocks from Nevada and eastern California—part II, western Nevada: Isochron/West, no. 4, p. 7–28.

Streckeisen, Albert, 1976, To each plutonic rock its proper name: Earth-Science Reviews, v. 12, p. 1–33.

Taggart, J.E., Jr., 2002, Analytical methods for chemical analysis of geologic and other materials: U.S. Geological Survey Open-File Report 02–0223, available at http://pubs.usgs.gov/of/2002/ofr-02-0223/OFR-02-0223.pdf.

U.S. Geological Survey, 2008, National geochemical database: Reston, Va., U.S. Geological Survey, available at http://mrdata.usgs.gov/ngdb/.

Appendix 1. Status and Treatment of Samples

Appendix 2. Petrographic Data for Rock Samples

Appendix 3. Geochemical Data for Rock Samples

Publishing support provided by:
Denver Publishing Service Center

For more information concerning this publication, contact:
Center Director, USGS Central Mineral and Environmental Resources Science Center

Box 25046, Mail Stop 973
Denver, CO 80225
(303) 236-1562

Or visit the Central Mineral and Environmental Resources Science Center Web site at:
http://minerals.cr.usgs.gov/

USGS

du Bray and others—**Petrographic and Geochemical Data for Cenozoic Volcanic Rocks, Bodie Hills, Calif. and Nev.**—Data Series 764 Version 1.1, August 2016

ISSN 2327-638X (online)
http://dx.doi.org/10.3133/ds764